Targeting pentamidine towards CD44-overexpressing cells using hyaluronated lipid-polymer hybrid nanoparticles

Ilaria Andreana[1] · Marta Chiapasco[1] · Valeria Bincoletto[1] · Sabrina Digiovanni[2] · Maela Manzoli[1] · Caterina Ricci[3] · Elena Del Favero[3] · Chiara Riganti[2] · Silvia Arpicco[1] · Barbara Stella[1*]

[1] Dipartimento di Scienza e Tecnologia del Farmaco, Università di Torino, Torino, Italy

[2] Dipartimento di Oncologia, Università di Torino, Torino, Italy

[3] Dipartimento di Biotecnologie Mediche e Medicina Traslazionale, Università di Milano, Milano, Italy

* Corresponding author: barbara.stella@unito.it

Abstract

Biodegradable nanocarriers possess enormous potential for use as drug delivery systems that can accomplish controlled and targeted drug release, and a wide range of nanosystems have been reported for the treatment and/or diagnosis of various diseases and disorders. Of the various nanocarriers currently available, liposomes and polymer nanoparticles have been extensively studied and some formulations have already reached the market. However, a combination of properties to create a single hybrid system can give these carriers significant advantages, such as improvement in encapsulation efficacy, higher stability, and active targeting towards specific cells or tissues, over lipid or polymer-based platforms. To this aim, this work presents the formulation of poly(lactic-*co*-glycolic) acid (PLGA) nanoparticles in the presence of a hyaluronic acid (HA)-phospholipid conjugate (HA-DPPE), which was used to anchor HA onto the nanoparticle surface and therefore create an actively targeted hybrid nanosystem. Furthermore, ionic interactions have been proposed for drug encapsulation, leading us to select the free base form of pentamidine (PTM-B) as the model drug. We herein report the preparation of hybrid nanocarriers that were loaded via ion-pairing between the negatively charged PLGA and HA and the positively charged PTM-B, demonstrating an improved loading capacity compared to PLGA-based nanoparticles. The nanocarriers displayed a size of below 150 nm, a negative zeta potential of -35 mV, a core-shell internal arrangement and high encapsulation efficiency (90%). Finally, the ability to be taken up and exert preferential and receptor-mediated cytotoxicity on cancer cells that overexpress the HA specific receptor (CD44) has been evaluated. Competition assays supported the hypothesis that PLGA/HA-DPPE nanoparticles deliver their cargo within cells in a CD44-dependent manner.

Graphical Abstract

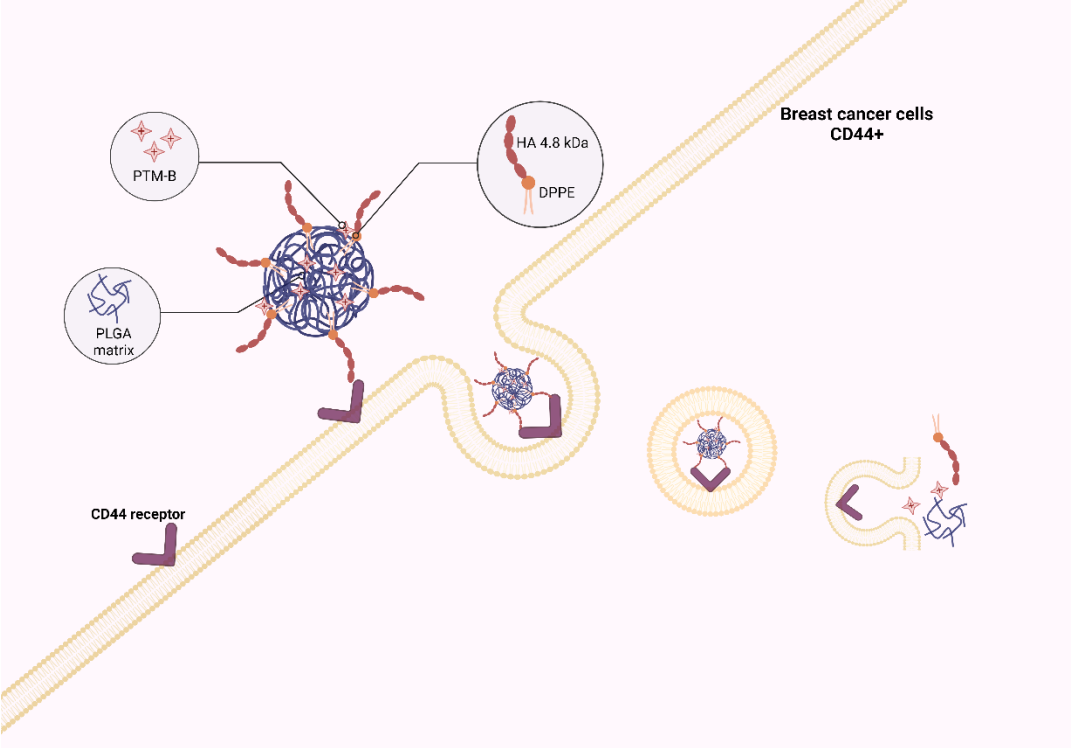

Keywords Lipid-polymer hybrid nanoparticles · PLGA · Hyaluronic acid · Phospholipid conjugate · Pentamidine

Introduction

Nanotechnology is a powerful strategy for the design of more effective and safer medical treatments and has significant applications against a plethora of pathologies, such as cancer and immune diseases [1, 2]. A number of different drug delivery systems (*e.g.*, polymer, lipid, inorganic) have been extensively studied for use in delivering active substances, ranging from small molecules, genetic material and biopharmaceuticals to diagnostic agents [3-5]. In the last few years, an increasing number of nanotechnology-based products have been marketed or have entered clinical trials, with these including liposomes, polymer and lipid nanoparticles [6-8]. The widespread use of sub-micronized structures as therapeutic carriers is largely attributed to their small size and their physicochemical properties, which can be managed to rationally design drug delivery systems that can reach different tissues in the body [9-11].

While other approaches do exist, advancements in improving nanocarrier properties can be achieved via the combining and blending of organic-organic or organic-inorganic materials. Indeed, tailor-made hybrid nanoparticles can display superior properties thanks to the combination of various materials with different chemical features and beneficial effects [12, 13]. For example, hybrid nanocarriers can co-encapsulate two cargos, enhance drug loading, improve physicochemical stability and targeting activity, and control drug release [14-16].

Of the organic materials that have been used to prepare nanocarriers, phospholipids and synthetic polymers are the most common. However, both present advantages and disadvantages. Lipid-based drug delivery systems have shown high biocompatibility, formulation simplicity, low toxicity, self-assembly properties and suitability for surface modification [17, 18]. Thanks to these properties and their similarity with biological membranes, lipid-based nanoparticles, in particular liposomes, have long been studied and used [19, 20]. Moreover, in recent years, lipid nanoparticles have been demonstrated to be a powerful tool for the delivery of mRNA-based vaccines and gene therapies [21, 22]. Nevertheless, drawbacks related to instability or poor bioavailability may hinder their clinical use [23, 24]. Alternatively, polymer nanoparticles, which are considered to be solid structures and are produced using natural or synthetic polymers that can be either lipophilic or hydrophilic, protect drugs from instability, and guarantee the encapsulation of hydrophobic and hydrophilic drug molecules. Their surface is generally thicker, stronger and more stable than that of other nanocarriers (*e.g.*, liposomes), thus stimulating additional interest for clinical applications. However, polymer nanoparticles may display toxicity and low drug loading capacity [25, 26].

In an effort to combine the biomimetic behavior of liposomes and the architectural advantages of polymers, multifunctional lipid-polymer hybrid nanoparticles have been proposed and have exploited

a huge variety of excipients that grant great opportunities for selective and efficient therapeutics delivery: in these systems, the polymer can control release, while the lipids may enhance loading efficiency and permeation [27, 28].

In this work, poly(lactic-*co*-glycolic) acid (PLGA) has been selected as a model hydrophobic biocompatible polymer to form the core of the hybrid nanoparticles. To set up an active targeting strategy, a hyaluronic acid (HA)-phospholipid conjugate (HA-DPPE) was added during nanoparticle preparation. The association of HA onto the surface of the nanoparticles was performed via the nanoprecipitation of PLGA into an aqueous solution of the HA-DPPE conjugate. PLGA/HA-DPPE nanoparticles were self-assembled, exposing HA on the surface and making it available for interaction with its principal cell surface receptor, CD44, which is overexpressed on a variety of tumor tissues, such as breast, ovarian and colon [29-31]. Following our previous approach in which drug association was based on electrostatic interactions with nanocarriers [32, 33], pentamidine (PTM), a diamine compound that is positively charged at physiological pH, was selected as the model drug. Already approved for antiparasitic therapy, it has recently been studied for its potential anticancer activity [34]. PTM was associated with lipid-polymer hybrid nanoparticles via ion-pairing between PTM free base (PTM-B) and negatively charged PLGA and HA. As a demonstration of HA ability to act as a targeting agent, the cytotoxicity of PTM-loaded hybrid nanoparticles was evaluated on breast cancer cell lines with low (MCF-7) and high (MDA-MB-231) CD44-receptor expression. Nanoparticle cell uptake was also studied on the latter cell line. Competition experiments were conducted to confirm the effect of the presence of HA on nanoparticle surface on cytotoxicity and cell uptake.

Materials and methods

Materials

PLGA (75:25, Resomer® RG 752 H, 4-15 kDa) (Fig. 1), pentamidine isethionate (PTM-I), 1,2-dipalmitoyl-*sn*-glycero-3-phosphoethanolamine (DPPE), Amicon Ultra-2 Centrifugal Filter Units (Ultracel®-50 kDa regenerated cellulose membrane, 2 mL) and solvents (analytical grade) were purchased from Merck (Milan, Italy). Sodium hyaluronate (HA) (4.8 kDa) was purchased from Lifecore Biomedical (Chaska, MN, USA). DPPE was conjugated to 4.8 kDa HA (HA-DPPE) (Fig. 1) using the method described by Arpicco *et al*. [29]. Filtered MilliQ® water (Millipore, Merck) was used. Solvents were evaporated using a rotating evaporator (Heidolph Laborota 400, Heidolph

Instruments, Schwabach, Germany) that was equipped with a vacuum pump (Diaphragm Vacuum Pump DC-4).

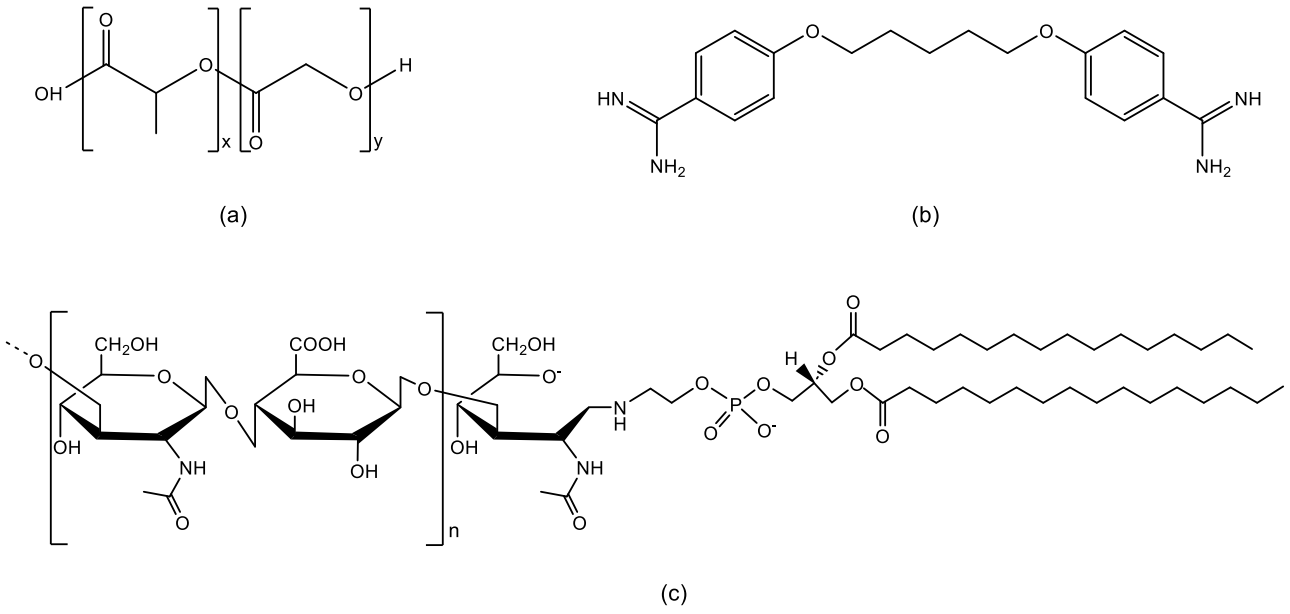

Fig. 1 Chemical structures of PLGA (a), PTM-B (b) and HA-DPPE (c)

Preparation and characterization of free base form of PTM

The free base form of PTM (PTM-B) (Fig. 1) was obtained via the addition of a 25% w/w NH_4OH solution at 4 °C to PTM-I dissolved in distilled water under magnetic stirring. The obtained precipitate was then filtered, washed three times with a 5% w/w NH_4OH solution and dried under vacuum conditions overnight. The conversion of PTM-I into PTM-B was confirmed by mass spectrometry analysis using electrospray ionization or by atmospheric pressure chemical ionization, in positive ion mode, on a Micromass ZQ spectrometer (Waters, Milan, Italy), as previously reported [35].

Preparation of lipid-polymer hybrid nanoparticles

Lipid-polymer hybrid nanoparticles were prepared using PLGA and the conjugate HA-DPPE via the nanoprecipitation technique [36]. To this aim, 6 mg of PLGA was dissolved in 500 µL of acetone, while 3.1 mg of HA-DPPE was added to 1 mL of MilliQ® water. Then, the acetone solution was added dropwise to the aqueous phase containing HA-DPPE under magnetic stirring. Nanoparticle formation occurred spontaneously without using any surfactant. After solvent evaporation under

reduced pressure, an aqueous nanoparticle suspension was obtained. PLGA and HA-DPPE were also nanoprecipitated alone as controls. PTM-B-loaded PLGA or PLGA/HA-DPPE nanoparticles were also prepared via the addition of an aliquot of an ethanolic stock solution of PTM-B (5 mg/mL) to the organic solution containing PLGA, for a maximum of 80 µg of PTM-B per mg of PLGA. The nanoparticle suspensions were purified using Amicon Ultra Centrifugal Filter Units (Ultracel®-50 kDa regenerated cellulose membrane, 2 mL). To this aim, the samples were centrifuged at 998 × g for 30 min and then at 111 × g for 10 min to remove the unincorporated drug and collect purified nanoparticles, respectively. Fluorescent PLGA or PLGA/HA-DPPE nanoparticles were prepared by adding 1.4 µg of the fluorescent probe Nile Red per mg of PLGA in the organic phase, before addition to the aqueous phase. The fluorescence of Nile Red-loaded nanoparticles at t_0, *i.e.* beside the incubation in cell culture, was measured fluorometrically, using the same procedure followed to measure the intracellular fluorescence, and did not differ more >5% from each batch. The particles were then stored at 4 °C until further use.

Physicochemical characterization of nanoparticles

The mean particle hydrodynamic diameter and polydispersity index (PDI) of the different nanoparticle samples were determined at 25 °C using quasi-elastic light scattering (QELS) on a nanosizer (Zetasizer Pro, Malvern Inst., Malvern, UK). The selected angle was 173° and the measurement was made after a 1/10 dilution of the particulate suspensions in MilliQ® water. The particle surface charge of the formulations was investigated via zeta potential measurements at 25 °C using the Smoluchowki equation and the Zetasizer Pro, after a 1/10 dilution of the suspensions in MilliQ® water. Each value is the average of three measurements carried out after independent experiments.

The physical colloidal stability of the nanoparticles under storage conditions (4 °C) was monitored by measuring mean hydrodynamic diameter, PDI and zeta potential by QELS at different time intervals for 28 days.

Field Emission Scanning Electron Microscopy (FESEM) was employed to investigate both the morphology and size of the PLGA/HA-DPPE nanoparticles. Images were collected by a Tescan S9000G FESEM 3010 microscope (Tescan Orsay Holding a. s., Brno-Kohoutovice, Czech Republic) working at 30 kV, equipped with a high brightness Schottky emitter, and fitted with Energy Dispersive X-ray Spectroscopy (EDS) analysis provided by an Ultim Max Silicon Drift Detector (SDD, Oxford, UK). For analyses, one drop of the prepared sample was deposited onto an aluminum stub that was coated with a conducting adhesive and subsequently left to dry in the air at room temperature. The

dried sample was submitted to Cr metallization (ca. 5 nm) using an Emitech K575X sputter coater (Quorumtech, Laughton, East Sussex, UK) to avoid charging effects and then inserted into the chamber by a fully motorized procedure. A histogram of the PLGA/HA-DPPE nanoparticle size distribution was obtained by considering a statistically representative number of particles, and the mean particle diameter (d_m) was calculated by applying the following equation:

$$d_m = \Sigma d_i ni / \Sigma n_i$$

where n_i is the number of particles of diameter d_i.

Counting was performed on electron micrographs obtained starting from 200,000 × magnification.

The amount of PTM-B incorporated into the PLGA and PLGA/HA-DPPE nanoparticles was determined indirectly by calculating the difference between the total amount of active compound added to the formulation and the amount of unincorporated drug after nanoparticle purification. To this aim, an aliquot of each formulation was purified using Amicon Ultra Centrifugal Filter Units at 998 × g for 30 min to collect the unincorporated drug. 200 µL of HCl 0.1 N was added to the unpurified nanoparticles and the filtrate, which were then freeze-dried for 24 h. The lyophilized product was then dissolved in 300 µL of dichloromethane. Methanol (2 mL) was then added, followed by centrifugation (3,992 × g for 15 min) to completely separate the precipitated PLGA polymer and HA-DPPE conjugate in unpurified nanoparticles [37]. The solutions obtained from the nanoparticle formulation and the filtrate were analyzed spectrophotometrically (DU 730 UV-vis spectrophotometer, Beckman Coulter, Brea, CA, USA) at 264 nm and the drug concentration was determined using a calibration curve, as already described [32]. Each sample was analyzed in triplicate. The results were expressed as encapsulation efficiency (EE) and drug loading (DL), calculated as follows:

Encapsulation efficiency (%) = [(total drug amount – free drug amount) / (total drug amount)] x 100

Drug loading (%) = [(total drug weight – free drug weight) / (total nanoparticle weight)] x 100

The internal arrangement of nanoparticles was investigated by Small Angle X-Ray Scattering (SAXS) technique. SAXS experiments have been performed at the ESRF Synchrotron (Grenoble, France) on ID02 beamline (dataset https://doi.org/10.15151/ESRF-ES-1351189712). Samples were put in capillaries (ENKI, Italy) mounted on a horizontal sample holder and irradiated with an X-ray beam with $\lambda = 0.1$ nm. Ten short frames (1 s) were acquired on each sample to avoid radiation damage. The

scattered X-ray intensity was acquired at two different sample-to-detector distances (1 m and 10 m) in the momentum transfer range $0.08 < q < 6$ nm^{-1}, being $q = 4\pi/\lambda(\sin\theta/2)$, where θ is the scattering angle. After angular regrouping and background subtraction, the intensity I(q) profile can give information on the shape and internal arrangement of the nanoparticles on a length-scale 1-600 nm. The form factors of the nanoparticles were modelled using SasView application [38].

PTM-B release from nanoparticles

To evaluate drug release from the PLGA and PLGA/HA-DPPE nanoparticles as a function of time, PTM-B-loaded nanosuspensions were placed into a dialysis tube (Spectra/Por® 3500 MWCO dialysis membrane, Spectrum) and then incubated at 37 °C in 10 mM phosphate-buffer saline (PBS) buffer pH 7.4 under sink conditions. Aliquots (500 µL, 6 mg/mL of PLGA) were withdrawn from the tube at predetermined time intervals (0, 1, 2, 5, 7, 24, 48, 72 h). The drug content was determined as previously described and compared with the initial value.

Cell lines

Human breast cancer MCF-7 and MDA-MB-231 cells were purchased from ATCC (Manassas, VA, USA). All cell lines were authenticated via microsatellite analysis using a PowerPlex kit (Promega Corporation, Madison, WI, USA; last authentication: March 2019). Cells were maintained in their respective media, which contained 1% v/v penicillin-streptomycin, with 10% v/v fetal bovine serum (FBS), in a humidified atmosphere at 37 °C.

Cytotoxicity

Cell viability was measured using the ATPlite Luminescence Assay System (PerkinElmer, Waltham, MA, USA), according to the manufacturer's instructions. To this aim, MCF-7 and MDA-MB-231 cells were incubated for 24, 48 and 72 h with a PTM-B ethanolic solution or the following nanoparticles: PLGA, PLGA/HA-DPPE, PTM-B-PLGA, PTM-B-PLGA/HA-DPPE (PTM-B concentration range: 10^{-7}-10^{-5} M). For the competition assays, cells were incubated for 72 h with PTM-B-loaded PLGA/HA-DPPE nanoparticles (PTM-B concentration: 10^{-5} M) in media containing a blocking anti-CD44 antibody (10 µL/mL) or free HA (100 µg/mL). Results were expressed as the percentage of viable cells relative to untreated cells, which were considered 100% viable.

Cellular uptake

1×10^8 cells were incubated with free Nile Red, Nile-Red-loaded PLGA or Nile-Red-loaded PLGA/HA-DPPE nanoparticles for 1, 6 and 24 h (fluorescent dye concentration: 10^{-5} M), then washed twice with PBS, detached with cell dissociation solution and rinsed with 300 µL PBS. The intracellular fluorescence, considered to be an index of nanoparticle uptake, was read on 1×10^4 cells using an EasyCyte Guava™ flow cytometer (Millipore), equipped with the InCyte software (Millipore). In order to achieve a quantitative measurement of intracellular uptake, the remaining 1×10^4 cells were resuspended in 350 µL PBS and a 50 µL aliquot was sonicated and used to measure the intracellular protein content with the BCA kit (Merck). The other cells were transferred to a 96-well plate and fluorescence was read using a Synergy HTX Multiple Reader (Bio-Tek Instruments, Winooski, VT, USA), using lambda excitation 549 nm and lambda emission 628 nm. The relative fluorescence units were transformed into nmoles of Nile Red, according to a previously set titration curve. For competition assays, cells were incubated for 24 h with Nile Red-loaded PLGA/HA-DPPE nanoparticles (fluorescent dye concentration: 10^{-5} M) in media containing a blocking anti-CD44 antibody (10 µL/mL) or free HA (100 µg/mL). Results were expressed as nmol/mg cell proteins.

Statistical analysis

All data in text and figures are presented as means ± SD. The results were analyzed using a one-way analysis of variance (ANOVA), on Statistical Package for Social Science (SPSS) software (IBM SPSS Statistics v. 19). $p < 0.05$ was considered statistically significant.

Results and discussion

Preparation and characterization of lipid-polymer hybrid nanoparticles

Although the HA-DPPE conjugate had previously been synthesized by our group to prepare HA-decorated liposomes for cutaneous administration or actively targeted towards CD44-overexpressing cancer cells [29, 39-42], it had only, to this point, been associated to polymer nanoparticles as a cryoprotectant agent to increase the long-term storage stability of empty nanocarriers, thus permitting the resuspension of PLGA nanoparticles after lyophilization. In that work, two HA molecular weights (4.8 kDa and 14.8 kDa) were tested for the association to the PLGA 75:25 matrix; however, only with

4.8 kDa HA we obtained stable, monodispersed nanoparticles with a mean diameter below 200 nm [43]. In this work, HA-DPPE has been associated to PLGA to obtain lipid-polymer hybrid nanoparticles actively targeted towards cancer cells. PLGA/HA-DPPE nanoparticles have also been loaded via the incorporation of the free base form of PTM (PTM-B) into the PLGA matrix in a single step via the nanoprecipitation technique, without the addition of a surface-active agent thanks to electrostatic interactions.

First, empty nanocarriers were obtained: the nanoparticles were prepared by solubilizing the HA-DPPE conjugate in the aqueous phase. During the addition of the PLGA organic solution, nanoparticles started forming and DPPE anchored to the polymer matrix thanks to its lipophilicity, while HA organized itself towards the aqueous phase, forming a hydrophilic outer shell. Unlike with liposomes, where HA-DPPE was added either during or after the formation of vesicles [41], the conjugate could only be added to PLGA nanoparticles during nanoprecipitation; the post-insertion strategy could not be used due to the rigid structure of the PLGA matrix after the formation of the nanoparticles. In fact, the addition of HA-DPPE to the pre-formed PLGA nanoparticles led to the precipitation of the nanosystem. It is worth noting that the nanoprecipitation of HA-DPPE alone (without PLGA) does not generate nanoparticles.

Compared to non-decorated PLGA nanoparticles, HA-coated nanosystems showed a higher mean diameter (125 nm *vs* 147 nm, respectively, despite a quite wide standard deviation for PLGA nanoparticles) suggesting that DPPE probably inserted into the surface layer of the polymer matrix; both formulations were monodispersed (Tab. 1). The presence of negatively charged HA on the surface slightly lowered the zeta potential value from -47 mV for PLGA nanoparticles to -55 mV for decorated nanocarriers.

Table 1

Physico-chemical characteristics (mean diameter, polydispersity index (PDI), zeta potential, initial PTM-B amount per mg of PLGA, encapsulation efficiency (E.E.) and drug loading (D.L.)) of nanoparticles (*n*=3).

Nanoparticles	mean diameter (nm) ± S.D.	PDI	zeta potential (mV) ± S.D.	max PTM added per mg of PLGA (µg)	E.E. (%)	D.L. (%)
PLGA	125 ± 20	0.08	-47 ± 4	-	-	-
PTM-B-PLGA	114 ± 14	0.10	-31 ± 2	30	83 ± 6	2.4 ± 0.2
PLGA/HA-DPPE	147 ± 6	0.06	-55 ± 12	-	-	-
PTM-B-PLGA/HA-DPPE	133 ± 15	0.05	-35 ± 1	80	90 ± 9	4.5 ± 0.4

FESEM characterization revealed that the PLGA/HA-DPPE nanoparticles have a round shape, in their as prepared form, and that they can be clearly observed as agglomerates embedded in the residual dried solution (Fig. 2A-B). Moreover, most of the PLGA/HA-DPPE nanoparticles have a size of below 200 nm, with 55% having a size of around 100 nm, as highlighted by the particle size distribution in Figure 2C. This is in good agreement with the mean particle hydrodynamic diameter reported in Table 1, although the dry size of the images is of course lower than the size of nanoparticles in solution. Moreover, the size distribution is number weighted, while in the scattering analysis it is intensity weighted. The calculated mean diameter is 94 ± 28 nm.

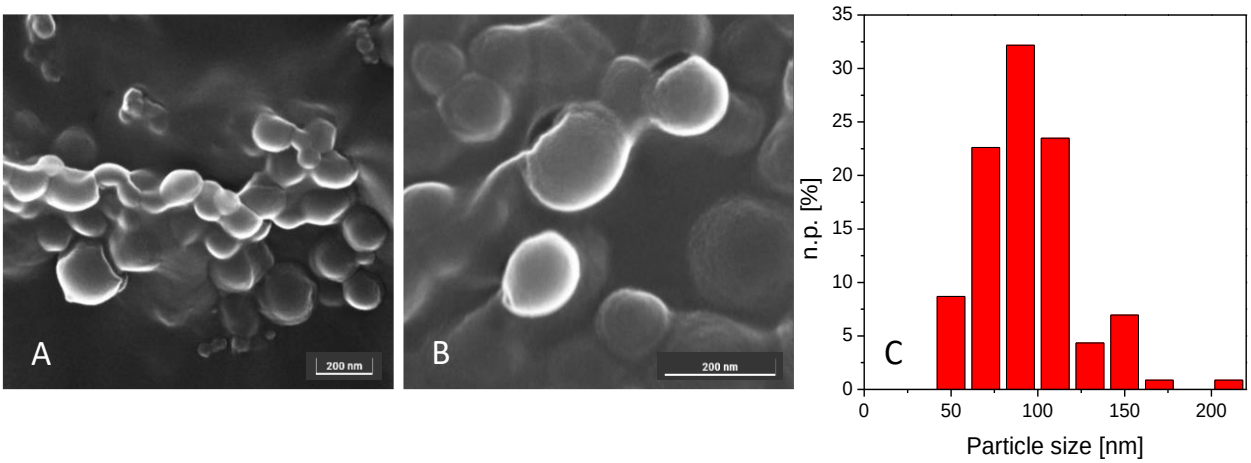

Fig. 2 Representative FESEM images of the prepared PLGA/HA-DPPE nanoparticles taken at different magnifications (A, B), and the corresponding particle size distribution (C). n.p. [%] represents the number of counted particles of diameter d_i. Images collected at 10 kV using the In-Beam SE detector. Instrumental magnification: 200,000 × and 400,000 ×, respectively.

To better incorporate the drug into the nanoparticle lipophilic matrix, the free base form of PTM was first obtained from the commercial, more hydrophilic isethionate salt. PTM-B was then dissolved in the acetone solution of PLGA before being added to the aqueous phase. The incorporation of PTM-B lowered the mean diameter of both the PLGA and PLGA/HA-DPPE nanoparticles, compared to their empty counterparts, by about 10% (Tab. 1); this can be ascribed to the ionic interactions occurring between the negatively charged PLGA carboxylic groups (pKa=4.5) and the positively charged PTM-B amidines (pKa=12). Indeed, in our previous works, we have shown that the spontaneous association between PTM-B and either PLGA or 1,1′,2-tris-norsqualenoic acid led to the stabilization of the nanocarriers, lowering the mean diameter [32, 33]. Here, due to the association of HA-DPPE, the mean diameter of the loaded hybrid nanoparticles is again higher than that of the non-decorated nanocarriers (133 nm *vs* 114 nm, respectively) (Tab. 1). All loaded suspensions were monodispersed. The zeta potential value was higher for both PTM-B-loaded formulations (PLGA and PLGA/HA-DPPE) than for the empty nanocarriers due to the presence of the positively charged drug,

which interacted with carboxylic groups (Tab. 1). The increase is more evident in the PLGA/HA-DPPE nanoparticles due to the presence of a higher quantity of associated drug.

The internal structure of nanoparticles was investigated by SAXS, suitable to assess the shape and the internal arrangement of particles from the hundreds of nms to the nms [44, 45]. The scattered intensity profiles of PLGA and PLGA/HA-DPPE nanoparticles at c = 6 mg/mL are reported in Figure 3. Measurements were also performed at lower concentrations (3 and 1.5 mg/mL) to verify the stability of nanoparticles upon dilution (Fig. S1). All the systems display the typical features of globular particles with a size of the order of one hundred nm, as visible in the low-q behavior of the spectra. The slope of the intensity decays at $q > 0.06$ nm^{-1} is proportional to q^{-4} as for well-defined interfaces between the particles and the solvent. Differences between the intensity profiles of the different systems can be observed mainly in the high-q region of the spectra, corresponding to short distances and thus to the local internal arrangement of nanoparticles. The best fit of I(q) for PLGA nanoparticles was obtained by modeling the particle form factor by a polydisperse sphere with a mean size of 120 ± 15 nm, in agreement with literature values [46] and light scattering results.

The intensity profile of PLGA/HA-DPPE nanoparticles was fitted by a core-shell spherical form factor. A spherical core, with an average radius of 58 ± 8 nm, is surrounded by a double-layered shell, the first layer, in contact with the core, has a thickness of 1.5 nm and is characterized by an electron density lower than the polymer core, as for lipids, while the external layer has a thickness of 3 nm and an electron density higher than the core, in agreement with the coating of the surface with a HA shell [47].

A core-shell spherical form factor was also used for the fit of PTM-B-loaded PLGA/HA-DPPE nanoparticles, with a smaller core (average radius 45 ± 7 nm) surrounded by a shell very similar to the unloaded system, with a slightly higher contrast of the most external layer.

Lipid-polymer hybrid nanoparticles were prepared using PLGA and the conjugate HA-DPPE through the nanoprecipitation technique. SAXS results show that this method led to the formation of nano-sized particles with a core-shell arrangement in the presence of HA-DPPE.

The loading of PTM-B did not affect dramatically the internal arrangement of the nanoparticles and contributed to keep the overall size around 120 nm. The reduction in the particle size and the slight effect observed by SAXS on the outer shell of loaded PLGA/HA-DPPE nanoparticles suggest the presence of PTM-B in the external part of the nanoparticles, contributing with the DPPE lipid chains to the stabilization of the polymeric core and interacting with HA on the external surface.

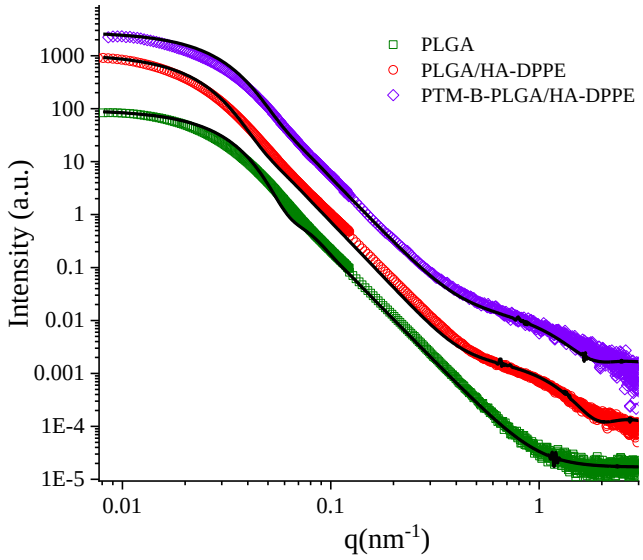

Fig. 3 SAXS spectra of nanoparticles (vertically shifted for better visibility) at c = 6 mg/mL: PLGA (green squares), PLGA/HA-DPPE (red dots), PTM-B-PLGA/HA-DPPE (violet diamonds). Black lines are the fitting curves.

Moving to drug incorporation, although both the loaded PLGA and PLGA/HA-DPPE nanoparticles displayed high EE values (83% and 90%, respectively) (Tab. 1), the amount of drug associated to the HA-decorated nanocarriers was 290% higher than that of the PLGA nanoparticles. The higher loading capacity of the hybrid nanoparticles suggests both an increase in the lipophilicity of the nanoparticle core, thanks to DPPE insertion, and the formation of additional ionic interactions between PTM-B and the carboxylic groups of HA, in agreement with SAXS results. This phenomenon led to an increased DL value (2.4% for PTM-B-PLGA *vs* 4.5% for PTM-B-PLGA/HA-DPPE nanoparticles). A similar approach has previously been exploited to form self-assembled ion pair-based nanoparticles with positively charged doxorubicin in the core and negatively charged hydrophilic HA in the outer shell [48].

In analyses of nanoparticle physical stability, no samples displayed precipitation/aggregation and/or significant increases in nanoparticle size over 4 weeks of storage at 4 °C.

Drug release from PLGA and hybrid nanoparticles was evaluated in PBS pH 7.4 at 37 °C (Fig. 4). Although the release profile is similar for both formulations, for loaded PLGA/HA-DPPE nanoparticles, an increased amount of PTM-B was released in the initial hours. This difference can be ascribed to the release of the drug molecules associated to the outer layer of HA, which occurs together with the diffusion of the drug from the polymer matrix and the erosion of PLGA.

We have previously demonstrated that the release profile of PTM-B is pH dependent when the drug is associated to a nanoparticle matrix via ionic interactions: at acidic pH, such as late endosomal or tumor environments, PTM-B is released more quickly from the polymer matrix than at pH 7.4 [33].

The pH-dependent drug release profile of PLGA/HA-DPPE nanoparticles may allow PTM-B to be selectively delivered to a tumor site thanks to association with the ligand HA, which is thought to target CD44-overexpressing cancer cells.

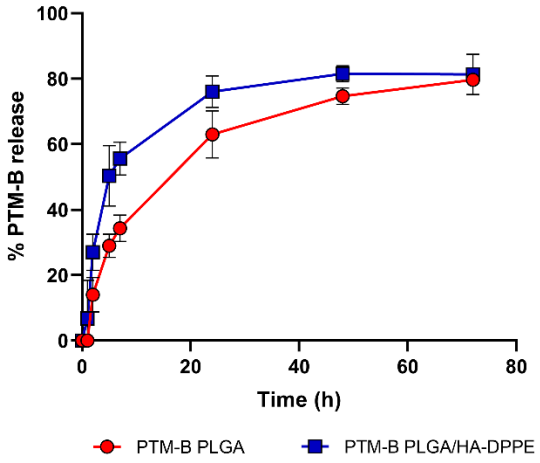

Fig. 4 PTM-B release from PLGA and PLGA/HA-DPPE nanoparticles as a function of time in PBS pH 7.4 at 37 °C.

Biological validation assays

Cell viability and PLGA/HA-DPPE nanoparticle uptake as mediated by the CD44 receptor in breast cancer cells

To validate our hypothesis as to the ligand-based intracellular delivery of PTM-B via PLGA/HA-DPPE nanoparticles, we performed the following *in vitro* assays. First, we measured the viability of MCF-7 cells, used as a CD44-negative cell line, and MDA-MB-231 cells, used as a CD44-expressing cell line [49], that were treated, in a dose- and time-dependent manner, with free PTM-B (Fig. 5A-F). In both cell lines, the free drug caused a similar decrease in cell viability excluding that the difference in cytotoxicity exerted by PTM-B may be attributed to the different levels of CD44. This pilot experiment also suggests that the MCF-7 and MDA-MD-231 cell pair is a good tool to compare the effects of untargeted (PLGA) and CD44-targeted (PLGA/HA-DPPE) PTM-B-loaded nanoparticles in terms of their internalization and toxicity. Neither the PLGA nor the PLGA/HA-DPPE empty nanocarriers reduced cell viability significantly (Fig. 5A-F), which demonstrates the good biocompatibility of the materials. When loaded with PTM-B, undecorated PLGA nanoparticles showed higher cytotoxic potential than free PTM-B, with no differences between MCF-7 and MDA-MB-231 being observed (Fig. 5A-F), which is to be expected because of the absence of an active

targeting moiety on the nanoparticle surface. While no differences in viability reduction were observed in the PTM-loaded HA-modified and undecorated PLGA particles in the CD44-negative cells (Fig. 5A, C, E), we found that the PTM-B-loaded PLGA/HA-DPPE nanoparticles were more cytotoxic than the free PTM-B and PTM-B-loaded PLGA nanoparticles in the CD44-expressing MDA-MB-231 cells (Fig. 5B, D, F). This result suggests that the presence of CD44 was the discriminating factor in mediating cytotoxicity, and that PTM-B was more easily delivered into the cells by PLGA/HA-DPPE nanocarriers. When we compared the effects of the PTM-B-loaded PLGA nanoparticles in MCF-7 *versus* MDA-MB-231, we found that the nanoparticles had greater effects in the latter. One possible explanation could rely on the different lipid plasma-membrane composition of the two cell lines. There was not any different composition in fatty acid (saturated fatty acid, mono- and poly-unsaturated fatty acid) compositions between the two cell lines, except for the saturated 16:0 fatty acid and the phospholipids phosphatidylinositol, phosphatidylserine and sphingomyelin that were slightly higher in MCF-7 cells [50]. These data may suggest a more rigid plasma-membrane of MCF-7 cells, less prone to PTM-B diffusion or PLGA nanoparticles endocytosis than MDA-MB-231 cells, thus explaining the higher effects obtained with: 1) PTM-B-loaded PLGA nanoparticles *versus* PTM-B; 2) PTM-B-loaded PLGA nanoparticles in MDA-MB-231 cells *versus* PTM-B-loaded PLGA nanoparticles in MCF-7 cells. We hypothesize that PTM-B-loaded PLGA nanoparticles have greater efficacy than PTM-B because of the higher delivery of PTM-B when uploaded into the nanocarriers. The above results led us to hypothesize an endocytosis-triggered mechanism. To support this hypothesis, we performed a competition assay, treating cells with the highest concentration of PTM-B-containing PLGA/HA-DPPE nanoparticles co-incubated with an excess of anti-CD44 blocking antibody or free HA at saturating amount [51]. Under these experimental conditions, viability was restored to control levels in the MDA-MB-231 cells, but not in the MCF-7 cells (Fig. 5E-F).

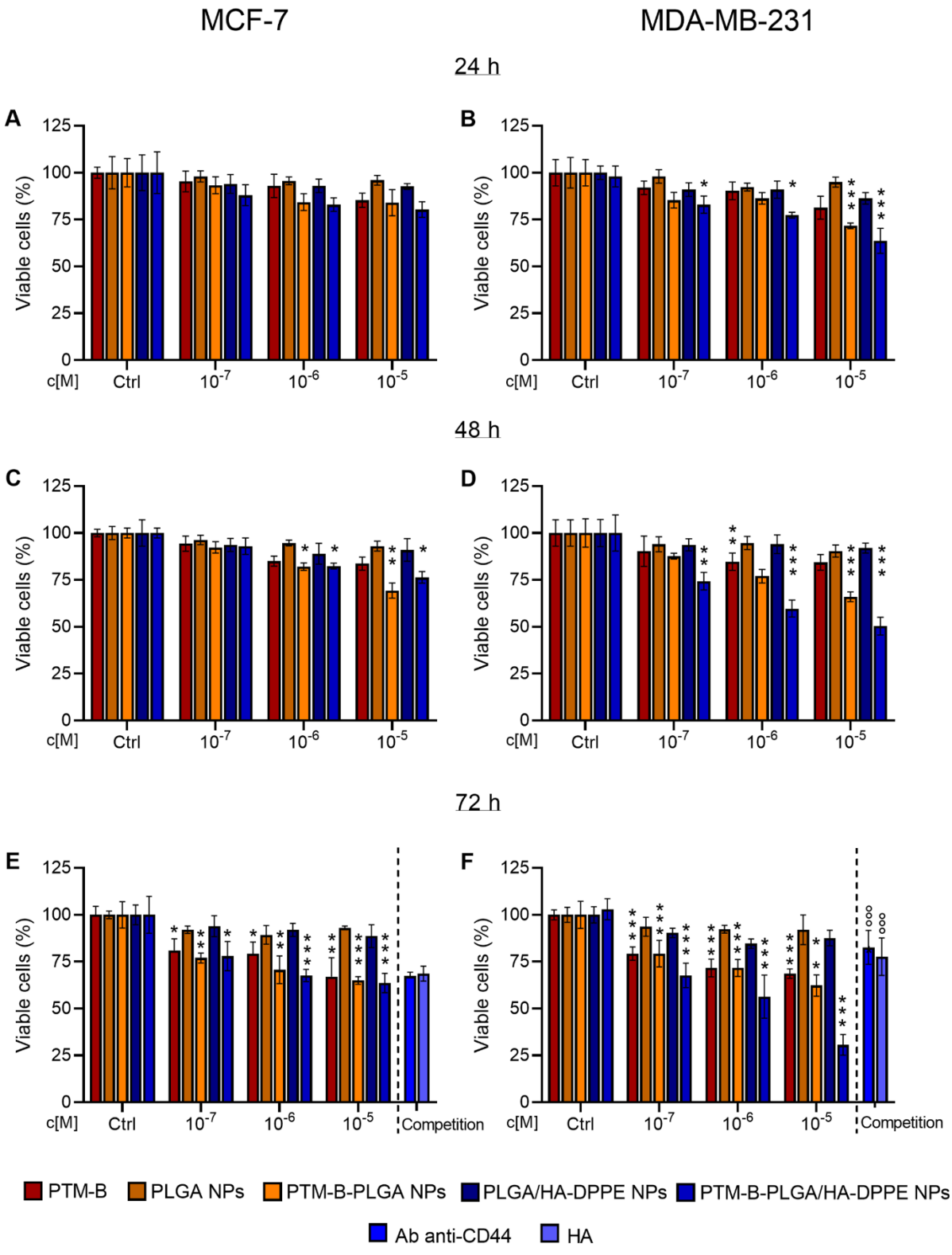

Fig. 5 Cell viability of MCF-7 (CD44-negative control) and MDA-MB-231 (CD44-positive control) cells incubated, for 24 (A-B), 48 (C-D) and 72 h (E-F), with increasing concentrations (10^{-7}, 10^{-6}, 10^{-5} M) of free PTM-B or the following nanoparticles: PLGA, PLGA/HA-DPPE, PTM-B-PLGA, PTM-B-PLGA/HA-DPPE. Ctrl: cells grown in fresh medium. Where indicated, cells were incubated for 72 h with PTM-B-loaded PLGA/HA-DPPE nanoparticles containing 10^{-5} M of PTM-B, in media containing a blocking anti-CD44 antibody (10 µL/mL) or free HA (100 µg/mL) (E-F). Data are means ± SD, in triplicate (*n*=3). Statistical significance *vs* respective control (Ctrl): *p<0.05, **p<0.01, ***p<0.001; Ab antiCD44/HA conditions *vs* PTM-B-loaded PLGA/HA-DPPE nanoparticles: °°°p<0.001.

To prove that cytotoxicity was mediated by the increased intracellular delivery of the PLGA/HA-DPPE nanoparticle cargo via CD44-mediated endocytosis, we measured the intracellular accumulation of fluorescently labeled PLGA/HA-DPPE nanoparticles in CD44-expressing MDA-MB-231 cells. As shown in Figure 6A-C, the uptake of Nile Red, Nile Red-loaded PLGA and Nile Red-loaded PLGA/HA-DPPE nanoparticles was time-dependent and followed this order: PLGA/HA-DPPE-carried dye > PLGA-carried dye > free dye. However, the intracellular uptake of Nile Red-loaded PLGA/HA-DPPE nanoparticles was prevented when CD44 was blocked by an inhibitory antibody or an excess of HA substrate, while this event did not happen with undecorated Nile Red-loaded PLGA nanoparticles (Fig. 6B-C). Both free Nile Red and Nile Red-loaded PLGA nanoparticles diffuse into the cells in a CD44-independent way. Therefore, it is expected that their uptake is similar in competition assays, where we did not inhibit the main route of entry. By contrast, Nile Red-loaded PLGA/HA-DPPE nanoparticles are endocytosed *via* CD44 receptor: therefore, when it is blocked by a neutralizing antibody or occupied by a saturating amount of HA, the main way of delivery for these nanoparticles is inhibited and the uptake of Nile Red-loaded PLGA/HA-DPPE nanoparticles resulted strongly reduced.

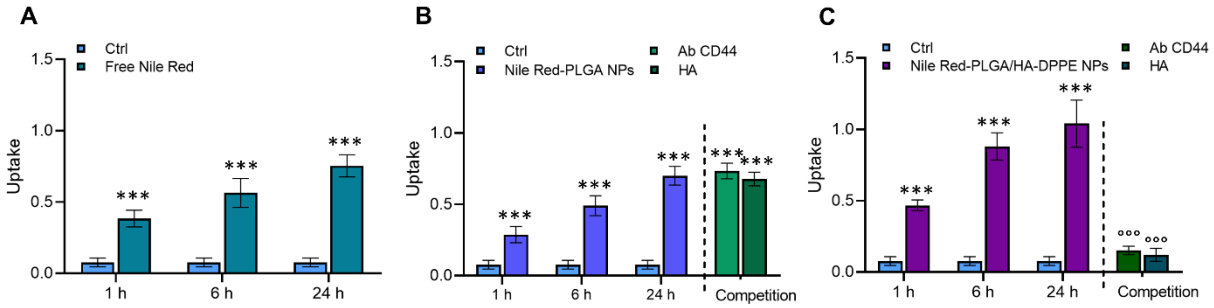

Fig. 6 Cellular uptake, expressed as nmol/mg cell protein, of free Nile Red (A), Nile Red-loaded PLGA nanoparticles (B) and Nile Red-loaded PLGA/HA-DPPE nanoparticles (C) (all containing 10^{-5} M of the dye), in MDA-MB-231, incubated for 1, 6 and 24 h. Ctrl: cells grown in fresh medium. Where indicated, cells were incubated for 24 h with Nile Red-PLGA/HA-DPPE nanoparticles containing 10^{-5} M of fluorescent dye, in media containing a blocking anti-CD44 antibody (10 µL/mL) or HA (100 µg/mL). Data are means ± S.D., in triplicate (n=3). Statistical significance *vs* respective control (Ctrl): ***p<0.001; *vs* Nile Red-loaded PLGA/HA-DPPE nanoparticles: °°°p<0.001. Nile Red-loaded PLGA/HA-DPPE *vs* Nile Red-loaded PLGA nanoparticles: §§p<0.01 (1 h), §§§p<0.001 (6 h, 24 h and competition).

The same trend of progressively increasing uptake and its being blocked by the anti-CD44 antibody or HA in excess was confirmed by flow cytometry experiments (Fig. 7A-B). These data strongly support the hypothesis that PLGA/HA-DPPE nanoparticles deliver their cargo within the cells in a CD44-dependent manner.

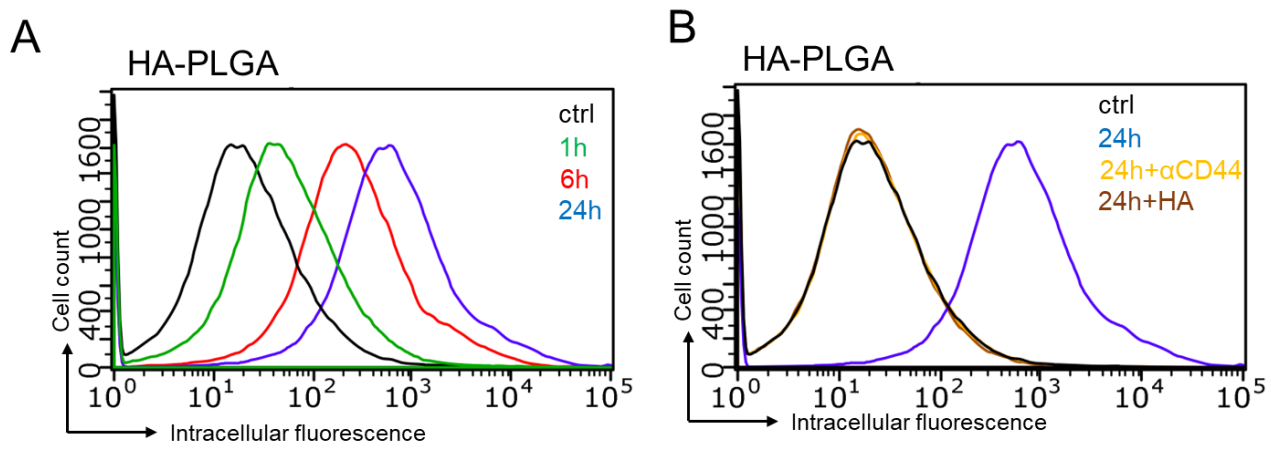

Fig. 7 Flow cytometry uptake. MDA-MB-231 cells were incubated for 1, 6 and 24 h in the absence (Ctrl) or in the presence of Nile Red-PLGA/HA-DPPE nanoparticles containing 10^{-5} M of the dye (A). Where indicated, cells were incubated for 24 h with Nile Red-PLGA/HA-DPPE nanoparticles containing 10^{-5} M of fluorescent dye, in media containing a blocking anti-CD44 antibody (10 µL/mL) or HA (100 µg/mL) (B). Representative histograms of three independent experiments.

These results may present translation potential. Indeed, MDA-MB-231 cells are a triple negative breast cancer (TNBC), one of the most aggressive breast cancer types. Chemotherapy based on doxorubicin and taxanes is currently the first treatment option, but tumors are very often chemoresistant, because of increased drug efflux, enhanced pro-survival/anti-apoptotic and stemness-related pathways [52]. The reduced uptake of chemotherapeutic drugs is another common cause of poor response [53]. Our PLGA-based system showed increased drug delivery within TNBC cells, representing a step forward in this direction. The association to HA further increases delivery by actively targeting CD44, a receptor that is often used in increasing drug delivery against breast cancer [54-56].

Drug repurposing is being considered to overcome resistance to conventionally used chemotherapeutics in TNBC treatment [57]. The anti-parasite drug PTM has been considered for drug repurposing in the oncological field, although it does not present strong cytotoxic potential when used alone. Its incorporation in actively targeted nanocarriers, such as PLGA/HA-DPPE nanoparticles, allows its intracellular uptake to be improved and may represent a promising strategy to enhance its cytotoxic potential.

Conclusion

The aim of the present work was to combine phospholipids and PLGA (previously separately used to prepare PTM-loaded liposomes and polymer nanoparticles) to obtain blended hybrid nanocarriers

actively targeted towards CD44-overexpressing cancer cells carrying a repurposed active molecule. We have made use of a phospholipid conjugate that was co-nanoprecipitated with PLGA as a versatile approach that avoids the chemical derivatization of the polymer matrix before or after nanoparticle formation, and that can be applied to different nanoparticle formulations. PTM-B was successfully loaded into PLGA and PLGA/HA-DPPE nanoparticles. However, the presence of HA in the lipid-polymer hybrid formulation drastically increased the amount of associated drug thanks to ionic interactions with HA carboxylic groups. Once characterized, the PTM-B-loaded nanocarriers were tested on cancer cells. *In vitro* results showed that PLGA/HA-DPPE nanocarriers are more cytotoxic on CD44-overexpressing cancer cells. Moreover, hybrid nanoparticles also showed higher intracellular accumulation in CD44-expressing MDA-MB-231 cells. CD44 endocytosis-mediated uptake was confirmed by competition assays in which the CD44 receptor was blocked. On these bases, further steps will involve the evaluation of the *in vivo* behavior of this system, notably pharmacokinetics and biodistribution, to develop this promising formulation for future applications.

Supplementary Information The online version contains supplementary material available at …

Acknowledgements The authors thank ESRF for financial support and beamtime (DOI: 10.15151/ESRF-ES-1351189712), ID02 staff for technical support and PSCM facility (Grenoble) for allowing on-site sample preparation. E.D.F. thanks BIOMETRA Dept. for partial support (PSR2021_DEL_FAVERO). This work benefited from the use of the SasView application.

Authors' contributions Conceptualization: Chiara Riganti, Silvia Arpicco, Barbara Stella; Methodology: Elena Del Favero, Chiara Riganti, Silvia Arpicco, Barbara Stella; Formal analysis and investigation: Ilaria Andreana, Marta Chiapasco, Valeria Bincoletto, Sabrina Digiovanni, Maela Manzoli, Caterina Ricci, Elena Del Favero; Writing - original draft preparation: Ilaria Andreana; Writing - review and editing: Sabrina Digiovanni, Maela Manzoli, Caterina Ricci, Elena Del Favero, Chiara Riganti, Silvia Arpicco, Barbara Stella; Supervision: Barbara Stella.

Funding The authors declare that no funds, grants, or other support were received during the preparation of this manuscript.

Availability of data and materials All data generated or analyzed during this study are included in this published article. Additional data related to this paper may be requested from the authors.

Declarations

Ethics approval and consent to participate Not applicable.

Consent for publication All authors approved the version to be published.

Competing interests The authors have no relevant financial or non-financial interests to disclose.

References

1. Mitchell, M.J., et al., *Engineering precision nanoparticles for drug delivery.* Nat Rev Drug Discov, 2021. **20**(2): p. 101-124.
2. Fan, Y.N., et al., *Progress in nanoparticle-based regulation of immune cells.* Med Rev (Berl), 2023. **3**(2): p. 152-179.
3. Zhang, P., et al., *Nbtxr3 radiotherapy-activated functionalized hafnium oxide nanoparticles show efficient antitumor effects across a large panel of human cancer models.* International Journal of Nanomedicine, 2021. **16**: p. 2761-2773.
4. Guo, B., et al., *Cuproptosis Induced by ROS Responsive Nanoparticles with Elesclomol and Copper Combined with αPD-L1 for Enhanced Cancer Immunotherapy.* Advanced Materials, 2023. **35**(22).
5. Rao, Z., et al., *Iron-based metal-organic framework co-loaded with buthionine sulfoximine and oxaliplatin for enhanced cancer chemo-ferrotherapy via sustainable glutathione elimination.* Journal of Nanobiotechnology, 2023. **21**(1).
6. Tenchov, R., et al., *Lipid Nanoparticles─From Liposomes to mRNA Vaccine Delivery, a Landscape of Research Diversity and Advancement.* ACS Nano, 2021. **15**(11): p. 16982-17015.
7. Park, H., A. Otte, and K. Park, *Evolution of drug delivery systems: From 1950 to 2020 and beyond.* J Control Release, 2022. **342**: p. 53-65.
8. Liu, Y., et al., *Nanoparticles advanced from preclinical studies to clinical trials for lung cancer therapy.* Cancer Nanotechnol, 2023. **14**(1): p. 28.
9. Ta, H.T., et al., *The effects of particle size, shape, density and flow characteristics on particle margination to vascular walls in cardiovascular diseases.* Expert Opin Drug Deliv, 2018. **15**(1): p. 33-45.
10. Li, X., et al., *Design of Smart Size-, Surface-, and Shape-Switching Nanoparticles to Improve Therapeutic Efficacy.* Small, 2022. **18**(6): p. e2104632.
11. Gamble, J.F., et al., *Morphological distribution mapping: Utilisation of modelling to integrate particle size and shape distributions.* Int J Pharm, 2023. **635**: p. 122743.
12. Sivadasan, D., et al., *Polymeric Lipid Hybrid Nanoparticles (PLNs) as Emerging Drug Delivery Platform-A Comprehensive Review of Their Properties, Preparation Methods, and Therapeutic Applications.* Pharmaceutics, 2021. **13**(8).
13. Jain, S., et al., *Lipid-Polymer Hybrid Nanosystems: A Rational Fusion for Advanced Therapeutic Delivery.* J Funct Biomater, 2023. **14**(9).
14. He, C., J. Lu, and W. Lin, *Hybrid nanoparticles for combination therapy of cancer.* J Control Release, 2015. **219**: p. 224-236.
15. Dehaini, D., et al., *Erythrocyte-Platelet Hybrid Membrane Coating for Enhanced Nanoparticle Functionalization.* Adv Mater, 2017. **29**(16).
16. Ferreira Soares, D.C., et al., *Polymer-hybrid nanoparticles: Current advances in biomedical applications.* Biomed Pharmacother, 2020. **131**: p. 110695.
17. Dhiman, N., et al., *Lipid Nanoparticles as Carriers for Bioactive Delivery.* Front Chem, 2021. **9**: p. 580118.

18. Yun, P., S. Devahastin, and N. Chiewchan, *Microstructures of encapsulates and their relations with encapsulation efficiency and controlled release of bioactive constituents: A review.* Compr Rev Food Sci Food Saf, 2021. **20**(2): p. 1768-1799.
19. Barenholz, Y., *Doxil®--the first FDA-approved nano-drug: lessons learned.* J Control Release, 2012. **160**(2): p. 117-34.
20. Adams, D., et al., *Patisiran, an RNAi Therapeutic, for Hereditary Transthyretin Amyloidosis.* N Engl J Med, 2018. **379**(1): p. 11-21.
21. Schoenmaker, L., et al., *mRNA-lipid nanoparticle COVID-19 vaccines: Structure and stability.* Int J Pharm, 2021. **601**: p. 120586.
22. Jia, Y., et al., *Lipid Nanoparticles Optimized for Targeting and Release of Nucleic Acid.* Adv Mater, 2023: p. e2305300.
23. Crommelin, D.J.A., P. van Hoogevest, and G. Storm, *The role of liposomes in clinical nanomedicine development. What now? Now what?* J Control Release, 2020. **318**: p. 256-263.
24. Hald Albertsen, C., et al., *The role of lipid components in lipid nanoparticles for vaccines and gene therapy.* Adv Drug Deliv Rev, 2022. **188**: p. 114416.
25. Ding, D. and Q. Zhu, *Recent advances of PLGA micro/nanoparticles for the delivery of biomacromolecular therapeutics.* Mater Sci Eng C Mater Biol Appl, 2018. **92**: p. 1041-1060.
26. Idrees, H., et al., *A Review of Biodegradable Natural Polymer-Based Nanoparticles for Drug Delivery Applications.* Nanomaterials (Basel), 2020. **10**(10).
27. Khalili, L., et al., *Smart active-targeting of lipid-polymer hybrid nanoparticles for therapeutic applications: Recent advances and challenges.* Int J Biol Macromol, 2022. **213**: p. 166-194.
28. Ghitman, J., et al., *Review of hybrid PLGA nanoparticles: Future of smart drug delivery and theranostics medicine.* Materials & Design, 2020. **193**: p. 108805.
29. Arpicco, S., et al., *Hyaluronic acid-coated liposomes for active targeting of gemcitabine.* Eur J Pharm Biopharm, 2013. **85**(3 Pt A): p. 373-80.
30. Zeng, X., et al., *pH-Responsive Hyaluronic Acid Nanoparticles for Enhanced Triple Negative Breast Cancer Therapy.* Int J Nanomedicine, 2022. **17**: p. 1437-1457.
31. de Paula, M.C., et al., *The role of hyaluronic acid in the design and functionalization of nanoparticles for the treatment of colorectal cancer.* Carbohydr Polym, 2023. **320**: p. 121257.
32. Stella, B., et al., *Pentamidine-Loaded Lipid and Polymer Nanocarriers as Tunable Anticancer Drug Delivery Systems.* J Pharm Sci, 2020. **109**(3): p. 1297-1302.
33. Andreana, I., et al., *Selective delivery of pentamidine toward cancer cells by self-assembled nanoparticles.* Int J Pharm, 2022. **625**: p. 122102.
34. Andreana, I., et al., *Nanotechnological approaches for pentamidine delivery.* Drug Deliv Transl Res, 2022. **12**(8): p. 1911-1927.
35. Peretti, E., et al., *Strategies to Obtain Encapsulation and Controlled Release of Pentamidine in Mesoporous Silica Nanoparticles.* Pharmaceutics, 2018. **10**(4).
36. Fessi, H., et al., *Nanocapsule formation by interfacial polymer deposition following solvent displacement.* International Journal of Pharmaceutics, 1989. **55**(1): p. R1-R4.
37. Mandal, T.K., et al., *Poly(D,L-lactide-co-glycolide) encapsulated poly(vinyl alcohol) hydrogel as a drug delivery system.* Pharm Res, 2002. **19**(11): p. 1713-9.
38. Doucet, M., et al., *SasView version 5.0.3. Zenodo. https://doi.org/10.5281/zenodo.3930098.* 2020.
39. Franze, S., et al., *Hyaluronan-decorated liposomes as drug delivery systems for cutaneous administration.* Int J Pharm, 2018. **535**(1-2): p. 333-339.
40. Cannito, S., et al., *Hyaluronated and PEGylated Liposomes as a Potential Drug-Delivery Strategy to Specifically Target Liver Cancer and Inflammatory Cells.* Molecules, 2022. **27**(3).
41. Franze, S., et al., *Rationalizing the Design of Hyaluronic Acid-Decorated Liposomes for Targeting Epidermal Layers: A Combination of Molecular Dynamics and Experimental Evidence.* Mol Pharm, 2021. **18**(11): p. 3979-3989.
42. Pandolfi, L., et al., *Liposomes Loaded with Everolimus and Coated with Hyaluronic Acid: A Promising Approach for Lung Fibrosis.* Int J Mol Sci, 2021. **22**(14).
43. Andreana, I., et al., *Freeze Drying of Polymer Nanoparticles and Liposomes Exploiting Different Saccharide-Based Approaches.* Materials (Basel), 2023. **16**(3).
44. Camara, C.I., et al., *Hyaluronic Acid-Dexamethasone Nanoparticles for Local Adjunct Therapy of Lung Inflammation.* Int J Mol Sci, 2021. **22**(19).

45. Di Cola, E., et al., *Novel O/W nanoemulsions for nasal administration: Structural hints in the selection of performing vehicles with enhanced mucopenetration.* Colloids Surf B Biointerfaces, 2019. **183**: p. 110439.
46. d'Angelo, I., et al., *Hybrid Lipid/Polymer Nanoparticles for Pulmonary Delivery of siRNA: Development and Fate Upon In Vitro Deposition on the Human Epithelial Airway Barrier.* J Aerosol Med Pulm Drug Deliv, 2018. **31**(3): p. 170-181.
47. Clementino, A.R., et al., *Structure and Fate of Nanoparticles Designed for the Nasal Delivery of Poorly Soluble Drugs.* Mol Pharm, 2021. **18**(8): p. 3132-3146.
48. Li, W., et al., *Hyaluronic acid ion-pairing nanoparticles for targeted tumor therapy.* J Control Release, 2016. **225**: p. 170-82.
49. Chang, G., et al., *CD44 targets Na(+)/H(+) exchanger 1 to mediate MDA-MB-231 cells' metastasis via the regulation of ERK1/2.* Br J Cancer, 2014. **110**(4): p. 916-27.
50. Corsetto, P.A., et al., *Effects of n-3 PUFAs on breast cancer cells through their incorporation in plasma membrane.* Lipids Health Dis, 2011. **10**: p. 73.
51. Cano, M.E., et al., *Synthesis of defined oligohyaluronates-decorated liposomes and interaction with lung cancer cells.* Carbohydr Polym, 2020. **248**: p. 116798.
52. Nedeljković, M. and A. Damjanović, *Mechanisms of Chemotherapy Resistance in Triple-Negative Breast Cancer-How We Can Rise to the Challenge.* Cells, 2019. **8**(9).
53. Muley, H., et al., *Drug uptake-based chemoresistance in breast cancer treatment.* Biochem Pharmacol, 2020. **177**: p. 113959.
54. Wang, L., et al., *Gold Nanomaterial System That Enables Dual Photothermal and Chemotherapy for Breast Cancer.* Pharmaceutics, 2023. **15**(9).
55. Mirzaei, S., et al., *Dual-targeted delivery system using hollow silica nanoparticles with H(+)-triggered bubble generating characteristic coated with hyaluronic acid and AS1411 for cancer therapy.* Drug Dev Ind Pharm, 2023: p. 1-10.
56. Abduh, M.S., *Anticancer Analysis of CD44 Targeted Cyclosporine Loaded Thiolated Chitosan Nanoformulations for Sustained Release in Triple-Negative Breast Cancer.* Int J Nanomedicine, 2023. **18**: p. 5713-5732.
57. Spini, A., et al., *Repurposing of drugs for triple negative breast cancer: an overview.* Ecancermedicalscience, 2020. **14**: p. 1071.